IBIC analysis of CdTe/CdS solar cells

IBIC analysis of CdTe/CdS solar cells.

E. Colombo[1,2], A. Bosio[3], S. Calusi[1,4], L. Giuntini[4], A. Lo Giudice, C. Manfredotti[1,2], M. Massi[4], P. Olivero[1,2], A. Romeo[5], N. Romeo[3] and E. Vittone[1,2]▪

[1] INFN, sezione di Torino, via P. Giuria 1, 10125, Torino, Italy.

[2] Experimental Physics Dept. and NIS excellence centre, University of Torino, via P. Giuria 1,10125, Torino, Italy.

[3] Physics Department, University of Parma, v.le G.P. Usberti 7/A, 43100, Parma, Italy.

[4] Physics Dept. University of Firenze and INFN Sezione di Firenze, Via Sansone 1, 50019, Sesto Fiorentino, Firenze, Italy.

[5] Science & Technology Dept. University of Verona, Ca Vignal 2, Strada Grazie 15, I-37134, Verona, Italy.

Abstract

This paper reports on the investigation of the electronic properties of a thin film CdS/CdTe solar cell with the Ion Beam Induced Charge (IBIC) technique. The device under test is a thin film (total thickness around 10 μm) multilayer heterojunction solar cell, displaying an efficiency of 14% under AM1.5 illumination conditions. The IBIC measurements were carried out using focused 3.150 MeV He ions raster scanned onto the surface of the back electrode. The charge collection efficiency (CCE) maps show inhomogeneous response of the cell to be attributed to the polycrystalline nature of the CdTe bulk material.

Finally, the evolution of the IBIC signal vs. the ion fluence was studied in order to evaluate the radiation hardness of the CdS/CdTe solar cells in view of their use in solar modules for space applications.

▪ corresponding author: Ettore Vittone, e-mail: vittone@to.infn.it

Classification codes and keywords

PACS:, 72.20.Jv; 41.75.Ak; 84.60.Jt;

Keywords: IBIC, thin film solar cell, charge collection efficiency.

Introduction

Thin film solar cells have the great advantage of being much easier to produce in comparison to crystalline silicon solar cells, giving a very high throughput with halved crystallization temperatures and monolithical interconnection.

In particular CdTe is particularly suitable for industrial mass production since it grows stoichiometrically with substrate temperatures above 250°C and can be successfully deposited with a large variety of techniques such as vacuum evaporation (VE), close space sublimation (CSS), vapor transport deposition (VTD), RF-sputtering, electro-deposition, screen printing, etc [1].

CdTe bandgap of 1.45 eV is very near to the theoretical maximum conversion efficiency (31%), while open circuit voltage and short circuit current are maximized. These substantial advantages have been proven by the impressive increase of CdTe photovoltaic modules production from a few MW in 2003 up to over 1 GW in 2008 with constantly decreasing production costs. Moreover, it has been shown that CdTe has the highest stability under proton and electron irradiation compared to the other photovoltaic devices, which makes CdTe cells very promising for space applications [2] .

The CdTe solar cells are structured in four different sections [1]. The front contact, which is the first layer deposited directly on the glass substrate, consisting of a transparent

conducting oxide (TCO), typically indium tin oxide (ITO) or tin oxide doped with fluorine (FTO); the CdS (also known as window layer), which is the n-type semiconductor of the junction and has to be optically transparent in order to allow the absorber to convert all the light spectrum; the CdTe, which has the double function of absorbing the light (giving place to the electron-hole pair generation) and to be the p-type semiconductor of the junction. Due to the high absorption coefficient of CdTe for photons in the visible range, the thickness of this layer is usually less than 10 μm. Finally, the back contact is typically a metal/metal or semiconductor/metal bi-layer.

In this paper we present the first IBIC characterisation of such thin film solar cell. The first motivation of this research is to demonstrate the feasibility of the IBIC technique to investigate the electronic properties of such thin film devices and to map their charge collection efficiency. The material is in fact polycrystalline and carrier traps and the electric field associated with grain boundaries will affect the motion of the carrier excess in the CdTe layer. With respect to other studies carried out with electron beam induced current measurements (EBIC) [3], the novelty of the use of energetic ions consists in the analysis of the bulk properties of the finite device.

Secondly, due to the interesting perspective of using such cells for space applications, we performed an investigation on the radiation hardness of cells under 3.150 MeV He ion bombardment through the continuous monitoring of the CCE vs. the ion fluences.

Experimental

The scheme of the multilayer CdS/CdTe cell that was fabricated by the Parma University group is shown in Fig. 1. The transparent contact is 500 nm indium tin oxide deposited by

DC-reactive sputtering at a substrate temperature of 300°C on soda lime glass; a 150 nm layer of zinc oxide is deposited by RF-sputtering at a substrate temperature of 200°C. The n-type material of the heterojunction is constituted by a 150 nm CdS layer which is deposited by RF-sputtering; the p-type side consists of a 8 μm thick CdTe layer deposited by close space sublimation at a temperature of 500°C. The junction is then activated by a recrystallization treatment of the CdTe, typically a "$CdCl_2$ treatment" that in our case consists in an annealing at 400°C in freon atmosphere. Finally the metal contact is a bi-layer of As_2Te_3:Cu (which gives the ohmic contact with CdTe) and Mo layer. The finished devices have typical conversion efficiencies between 14 and 15 % [4]. The lateral dimensions of the cell under investigation are (4.4x4.4 mm^2).

Since at low bias voltage the reverse current was of the order of fractions of μA, resulting in an high noise level at the input of the preamplifier, IBIC measurements were carried out without any applied bias voltage.

Silver paste was used to bond an Au wire for the connection of the Mo electrode to an Amptek A250 charge sensitive preamplifier and the ITO transparent electrode to ground. The charge signal was amplified with a shaping amplifier (from Silena 761) and fed into an OM-DAQ acquisition system. At zero bias the capacitance of the cell is more than 100 pF which corresponds to an equivalent noise energy of about 88 keV as evaluated from the FWHM of the signal from a precision pulse generator.

The IBIC measurements were performed at the external scanning ion microprobe facility installed at the 3 MV Tandem Accelerator [5] at the Laboratorio di Tecniche Nucleari per i Beni Culturali (LABEC) in Florence (I).

A 3150 keV He beam was extracted in air through a silicon nitride (Si_3N_4) window (50 nm thick, 1 mm^2 area) and focused and raster scanned by means of an Oxford Microbeam system over the Mo surface of the cell. The window is inclined of 60° with respect to the beam axis, and the sample was located as close as possible to the exit window (Fig. 2). The measurement were performed in air; according to SRIM simulation [6], the energy of the ions transmitted through the Si_3N_4 window and the 1 mm thick air layer interposed between the sample and the centre of the exit window was 3000 keV with a FWHM of 11 keV and the lateral straggling of the beam was about 4 μm in FWHM. The average energies of the ions at the opposite corners of the windows are 3041 keV and 2965 keV and the relevant FWHM are 14 and 18 keV, respectively. These values fall within the equivalent noise energy level (88 keV) of the electronic chain.

In the following, CCE is reported in terms of pulse height or collected charge and not as the ratio of the collected charge to the generated one. This is due to the difficulties in evaluating the electron/hole pair generation energy for all the materials stacked in the multilayer structure.

Results and discussion

Fig. 3 shows an IBIC map of the CdTe/CdS solar cell. The black region on the top side is due to the silver paste used for bonding. In average, about 20 pulses were collected at each pixel and the map was obtained encoding the median of the charge pulse height distribution in a grey scale; the histogram of the pixel distribution vs. the pulse height is shown in Fig. 4, as resulting from the processing of the total scan recorded in event-by-

event mode. As expected, the pixel distribution is much more peaked than the total pulse spectrum shown in the same figure.

The IBIC signal encoded in Fig. 3 represents the charge induced at the sensing electrode by the motion of free carriers created by ionization. It is worth noticing that the generation profile extends all over the sample thickness (Fig. 5), hence, the median signal accounts both for the drift of carriers generated into the active region (where electric field occurs) and to the injection of minority carriers (electrons) moving by diffusion from the neutral region [7]. However, we were not able to evaluate the relative weights of the drift and diffusion contributions on the total induced charge due to the difficulties in estimating the depletion layer extension of the multilayer structure.

The non-homogeneities shown in Fig. 3 can be attributed to the polycrystalline nature of the CdTe layer. In the zoomed (100x100 μm^2) region reported in the inset, structures showing higher CCEs have dimensions of the order of 10 μm, surrounded by darker (i.e. low efficiency) boundaries.

Since the dimension of the features in the IBIC maps is comparable to the size of the CdTe microstructures after $CdCl_2$ re-crystallization, the attribution of the dominant role of grain boundaries in the limitation of the carrier drift lengths appears very convincing. In fact, in analogy with what has been extensively reported after IBIC studies on polycrystalline CVD diamond [8] and, recently, on polycrystalline CdTe radiation detectors [9], grain boundaries act as preferential regions where recombination or trapping occurs, and the contrast in the IBIC image highlights grain shapes in the bulk material.

In order to evaluate the sensitivity of the cell to ion damage, a 100x100 μm^2 area was scanned by the He beam up to a total fluence of $2x10^{10}$ ions·cm^{-2}. After this selective irradiation, this area presents a lower charge collection efficiency with respect to the pristine regions, as shown in Fig. 6. Clearly, the ion bombardment induces damage in the material, generating recombination centres, resulting in a decrease of the induced charge signal. In order to analyse the variation of the charge pulse height with cumulative fluence, IBIC spectra and maps were taken at regular fluence intervals during the irradiation. From the analysis of the spectra, a decrease of the average pulse height vs. the ion fluence is evident. This effect is represented in the spectra (obtained by the processing of 2000 pulses uniformly distributed onto the irradiated area) of Fig. 7 at four different fluences, and summarised in Fig. 8, where the average pulse height is reported as function of ion fluence. In the same graph the behaviour of the standard deviation of the pulse height distribution is also reported, which highlights the increasing uniformity (i.e. decreasing dispersion) of the response as the fluence increases. This is further confirmed by the maps in Fig. 9. High efficiency grains observable after small ion fluences disappear in the maps relevant to more damaged regions, which present lower contrast.

Conclusions

This paper presents the first IBIC characterisation of a CdTe/CdS multilayer solar cell. The experiments were carried out using a 3.150 He ion beam extracted in air and focused onto the back electrode of the solar cell. Despite the employment of an extracted beam in air, the spatial resolution of the IBIC maps was proven to be adequate to resolve the

polycrystalline structure of the bulk materials, highlighting the role played by grain boundaries to limit the drift lengths of carriers.

Damage effects induced by ion irradiation were evaluated by analysing the average IBIC signal coming from a 100x100 μm^2 region irradiated up to a fluence of $2 \cdot 10^{10}$ ions/cm^2. The average pulse height decreases of 20% with respect to the pristine case; the analysis of the maps recorded at different fluences shows that the decreasing of CCE is not uniform; in fact large grains, showing higher efficiencies in the pristine case, are more sensitive to radiation effects. As a consequence, ion irradiation levels levels the response of the cell towards low CCE values, reducing the spatial fluctuations as indicated microscopically by the decreasing contrast of IBIC maps.

Acknowledgements

This work has been carried out and financially supported in the framework of the INFN experiment “DANTE”.

References

[1] A. Romeo, M. Terheggen, D. Abou-Ras, D. L. Bätzner, F.-J. Haug, M. Kälin, D. Rudmann, A. N. Tiwari, Progress in Photovoltaics: Research and Applications, 12 (2-3) (2004): 93.

[2] D.L.Batzner, A.Romeo, M.Terheggen, M.Dobeli, H.Zogg, A.N.T Iwari, Thin Solid Films 451–452 (2004) 536–543.

[3] S.A. Galloway, P.R. Edwards, K. Durose, Solar Energy Materials & Solar Cells 57 (1997), 61-74

[4] N. Romeo, A. Bosio, S. Mazzamuto, A. Romeo, L. Vaillant-Roca. Proceedings of the 22nd Eu-PVSEC, Milan, Italy, 2007, p. 1919.

[5] L. Giuntini, M. Massi, S. Calusi, Nucl. Instr. and Meth. in Phys. Res. A, 576, (2007) 266-273.

[6] J.F. Ziegler, SRIM - The Stopping and Range of Ions in Matter (version 2008.04), Available from: <http://www.srim.org/>.

[7] M. B. H. Breese, E. Vittone, G. Vizkelethy, P. J. Sellin, Nucl. Instr. and Meth. in Phys. Res. B 264 (2007) 345–360.

[8] P. Olivero, C. Manfredotti, E. Vittone, F. Fizzotti, C. Paolini, A. Lo Giudice, R. Barrett, R. Tucoulou, Spectrochimica Acta Part B 59 (2004) 1565– 1573 and references therein.

[9] N. Baier, A. Brambilla, G. Feuillet, A. Lohstroh, S. Reneta, P. Sellin, Nucl. Instr. and Meth. in Phys. Res. A: 576, (2007), 5-9.

Figure Captions

Fig. 1 Scheme of the CdTe/CdS cell, with the relevant electrical connections.

Fig. 2 Scheme of the exit window – sample geometry. The dimension of the Si_3N_4 window is 1x1 $mm^{2.}$.

Fig. 3 IBIC map of the CdTe/CdS solar cell. In the inset, a zoom of the map (100x100 μm^2)

Fig. 4 Pulse height frequency histogram (right vertical scale) and pixel distribution (left vertical scale) relevant to the map in the previous figure. The pixel distribution was evaluated considering a pulse threshold at channel 150.

Fig. 5 SRIM [6] simulation of the energy loss profile of 3 MeV He ions in the multilayer CdTe/CdS solar cell.

Fig. 6 IBIC map of the solar cell after the selective irradiation of the area highlighted in the inset in Fig. 3.

Fig. 7 Spectral evolution of the average IBIC signals recorded after different ion fluences. The measured charge was evaluated by normalising the pulse response by a Si barrier detector used as reference.

Fig. 8 Average pulse height (left scale, full square) and standard deviation (right scale, open circle) vs. ion fluence. Data are normalised to the pristine case.

Fig. 9 IBIC maps of the irradiated region after different fluences.

Fig.1

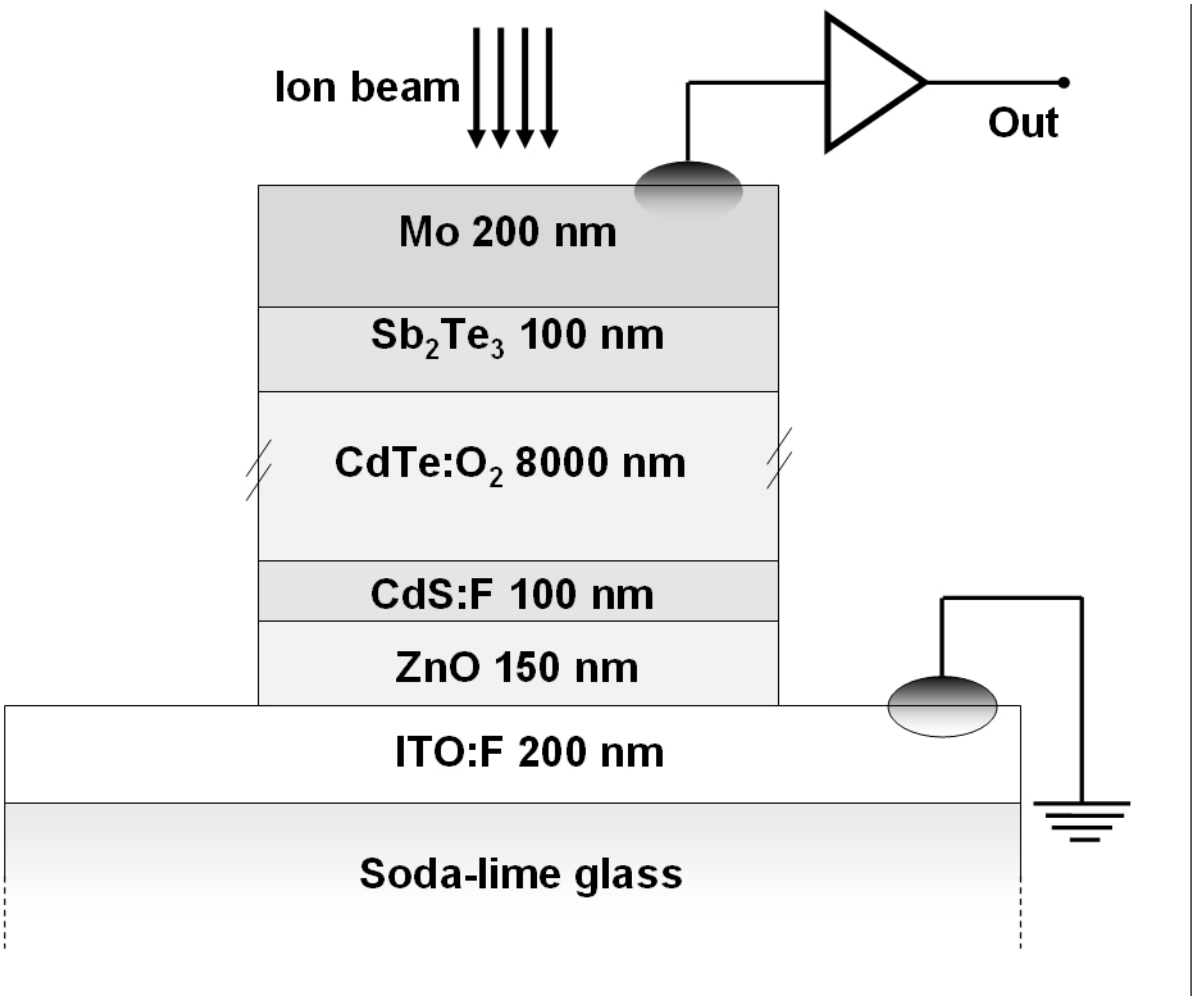
Ion beam
Out
Mo 200 nm
Sb2Te3 100 nm
CdTe:O2 8000 nm
CdS:F 100 nm
ZnO 150 nm
ITO:F 200 nm
Soda-lime glass

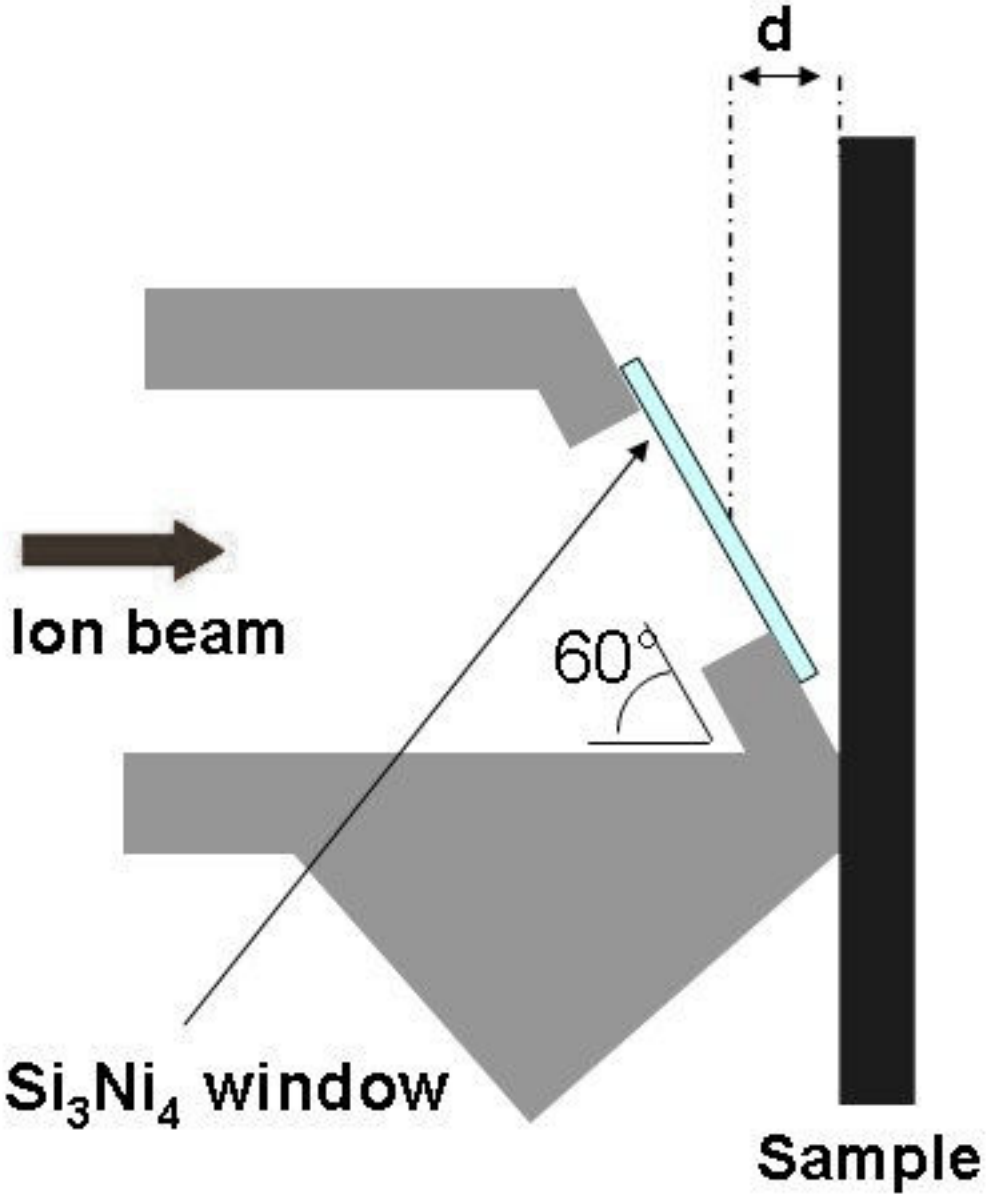

Fig. 2

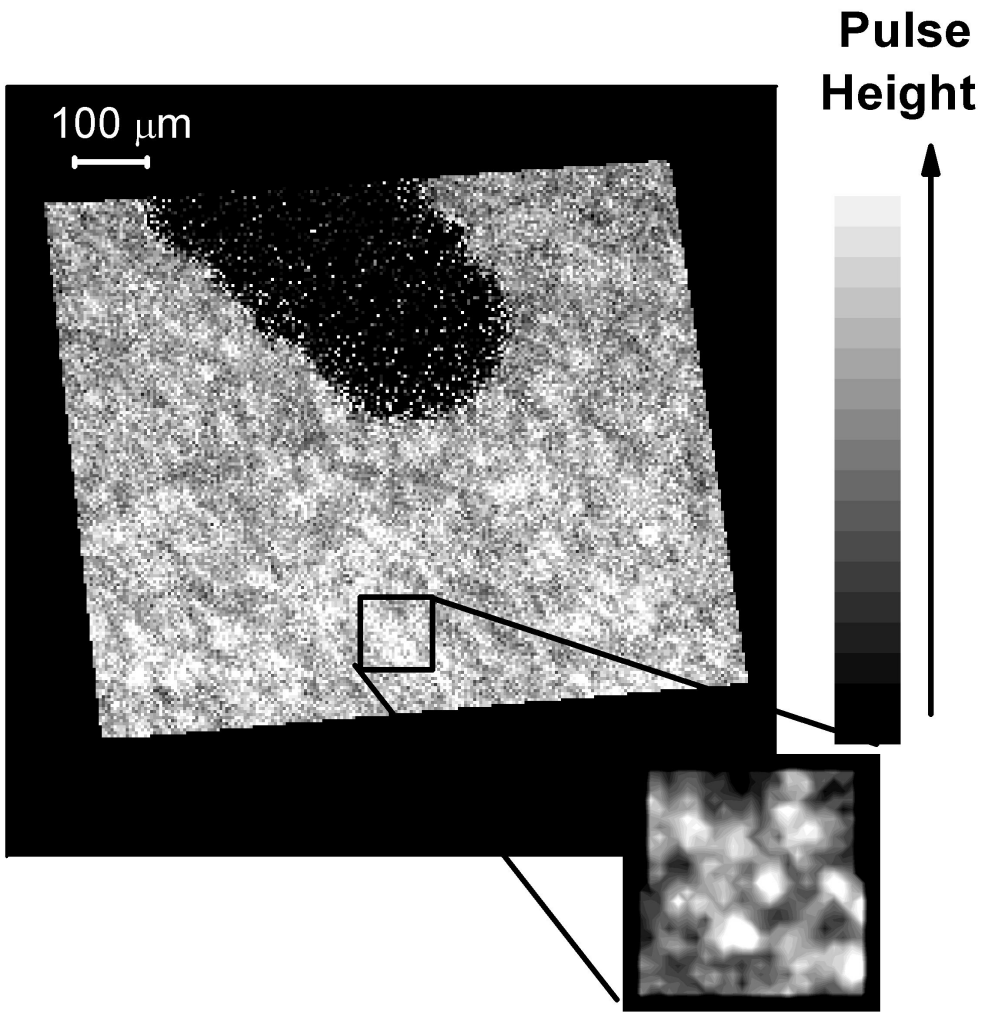

Fig. 3

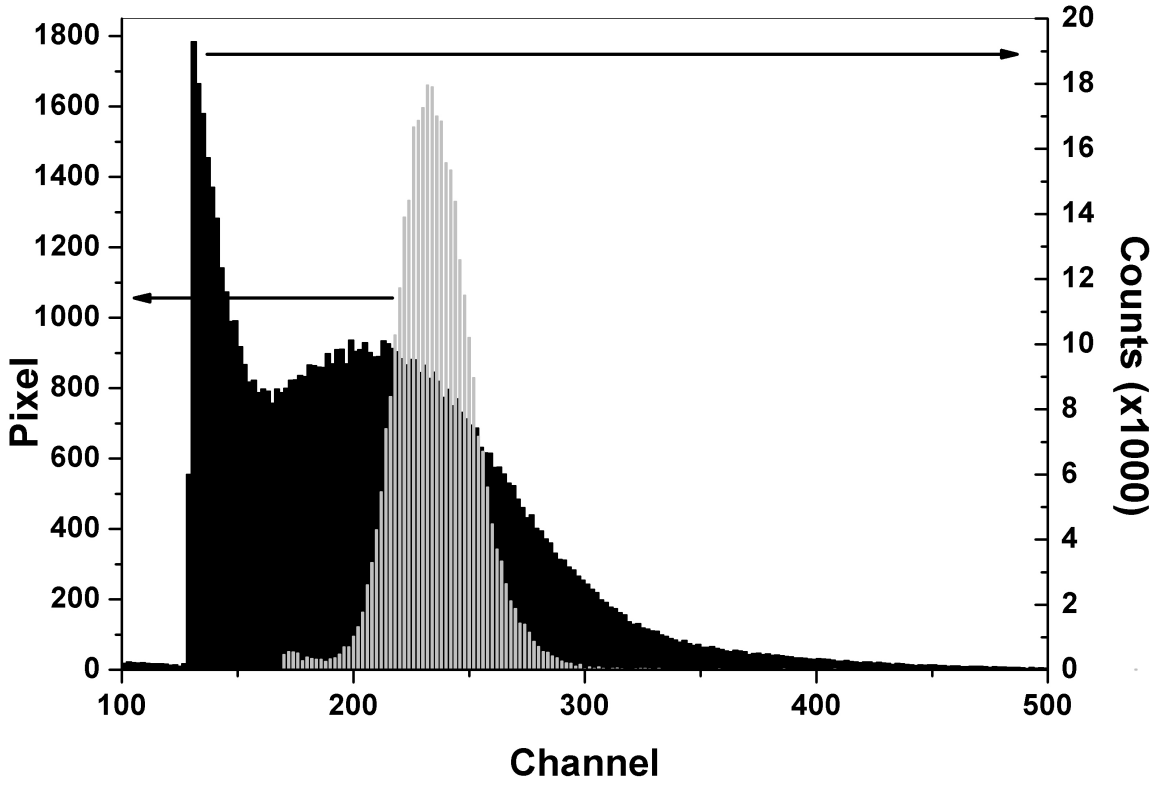
Pixel
Counts (x1000)
Channel
1800
1600
1400
1200
1000
800
600
400
200
0
20
18
16
14
12
10
8
6
4
2
0
100
200
300
400
500

Fig. 4

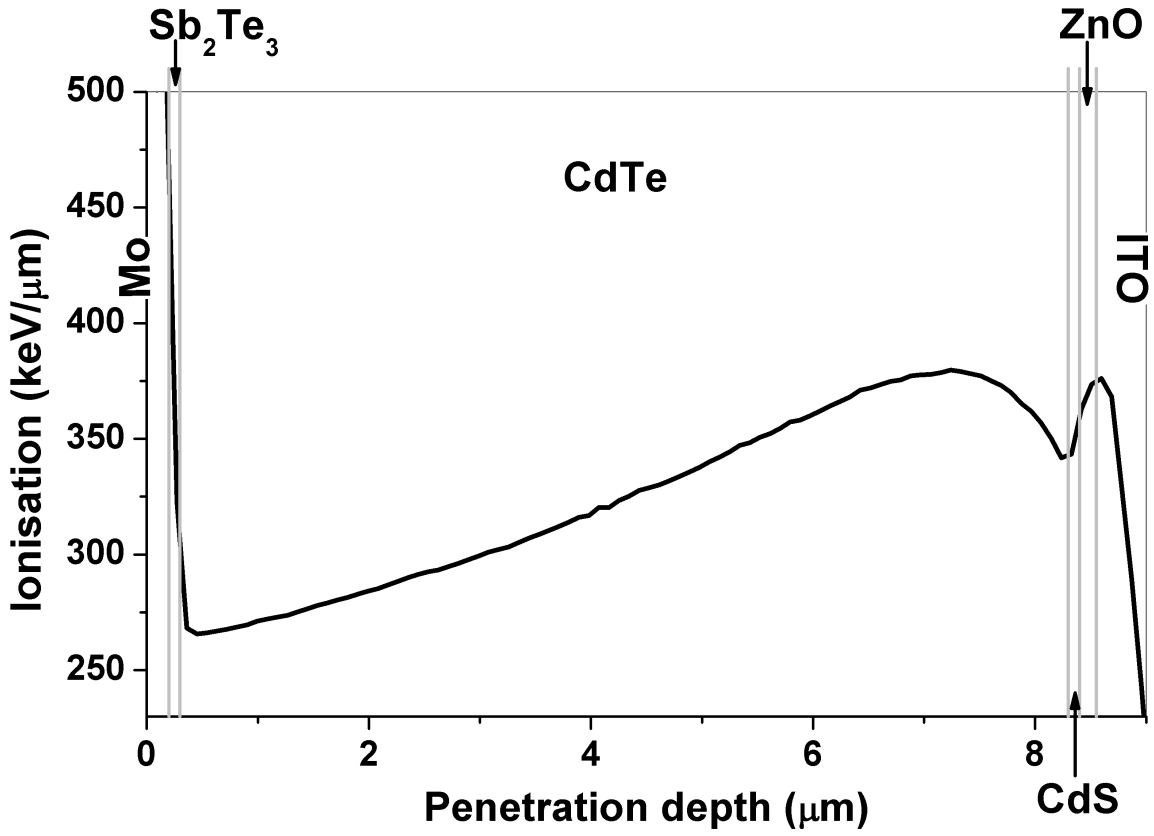
Sb2Te3
ZnO
CdTe
Mo
ITO
Ionisation (keV/μm)
500
450
400
350
300
250
0
2
4
6
8
Penetration depth (μm)
CdS

Fig. 5

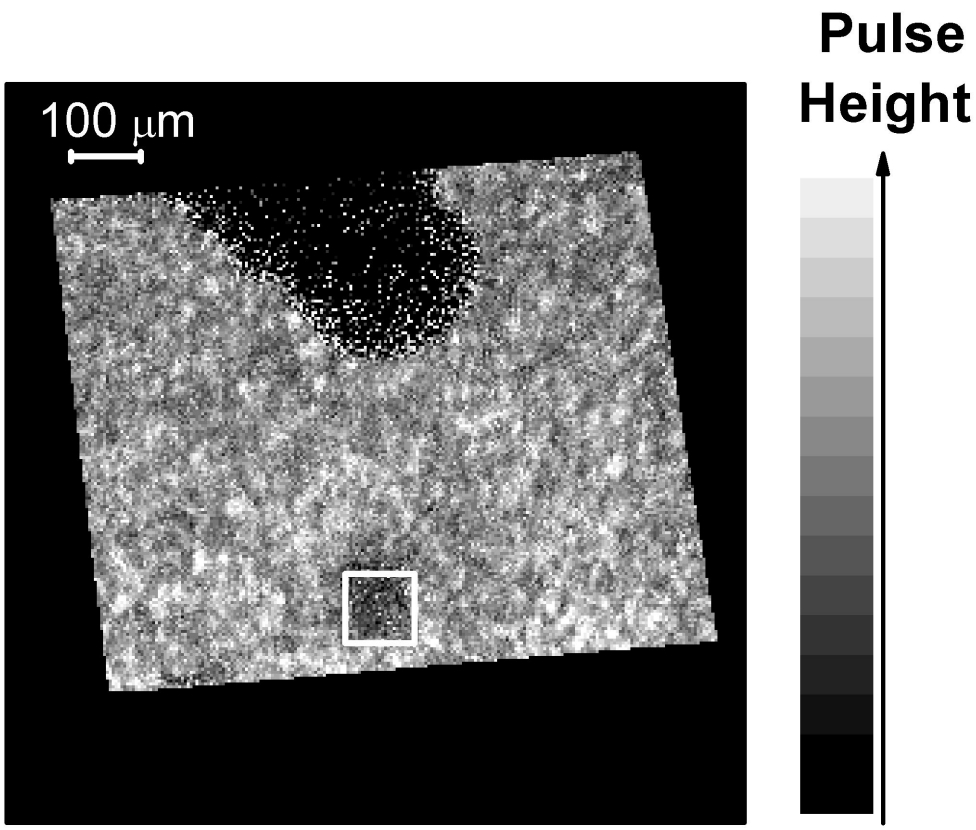

Fig. 6

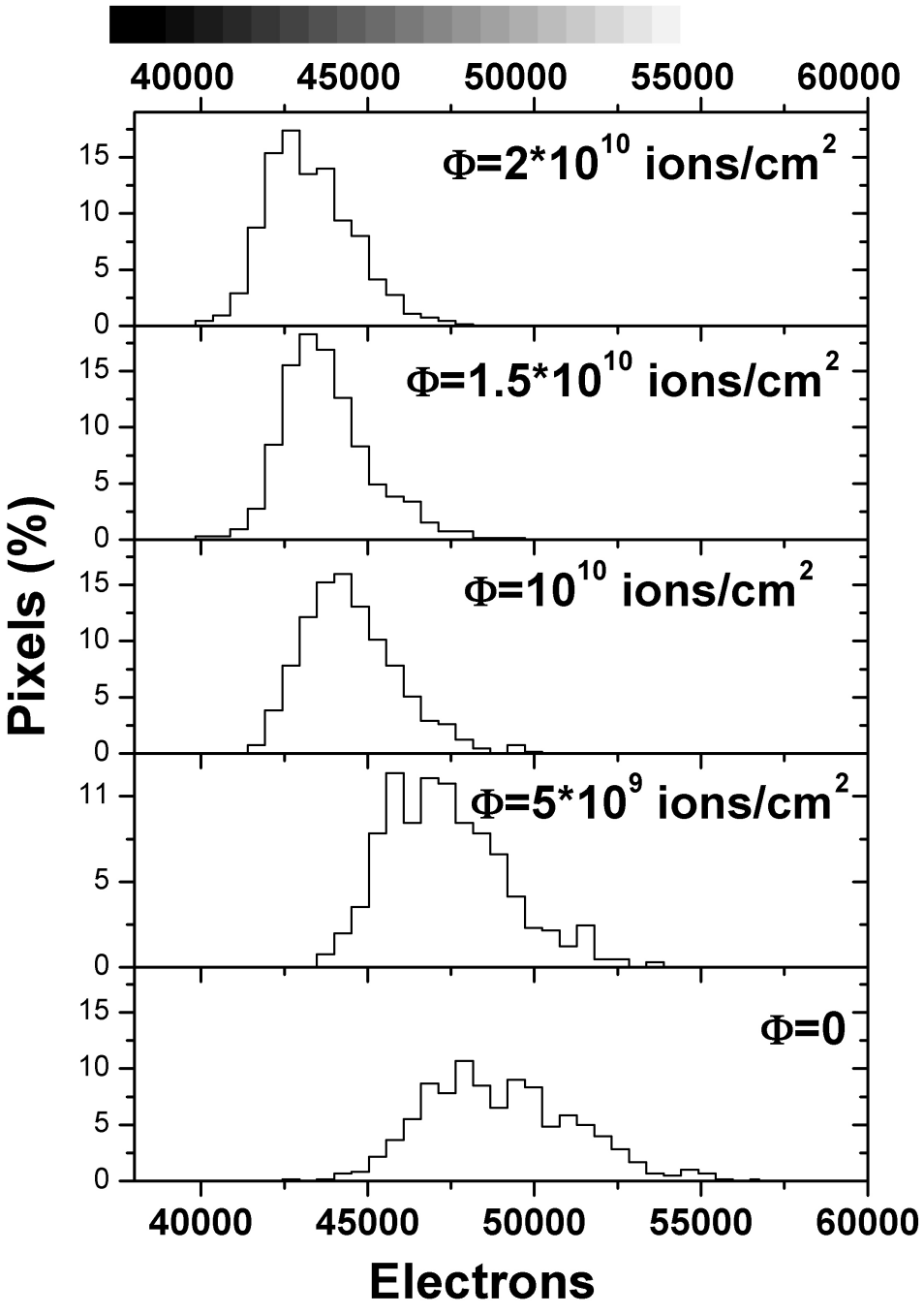
40000
45000
50000
55000
60000
Φ=2*10^10 ions/cm^2
Φ=1.5*10^10 ions/cm^2
Φ=10^10 ions/cm^2
Φ=5*10^9 ions/cm^2
Φ=0
Pixels (%)
Electrons

Fig. 7

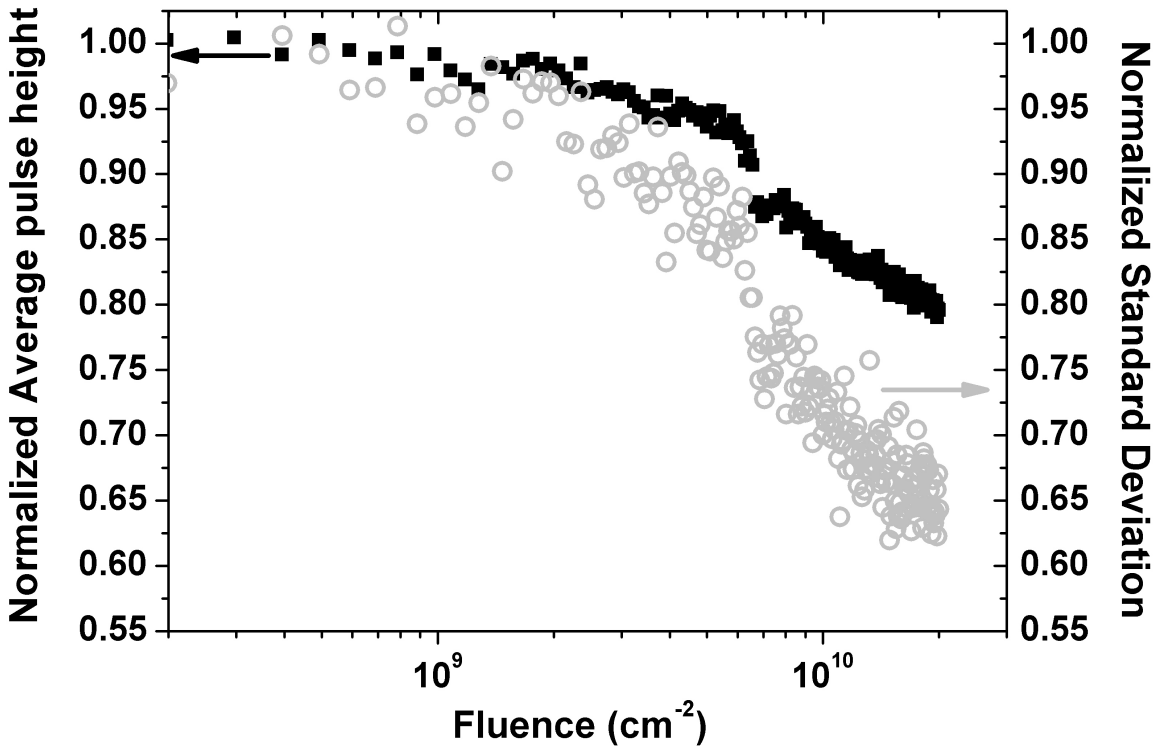
Normalized Average pulse height
Normalized Standard Deviation
1.00
0.95
0.90
0.85
0.80
0.75
0.70
0.65
0.60
0.55
10^9
10^{10}
Fluence (cm^{-2})

Fig. 8

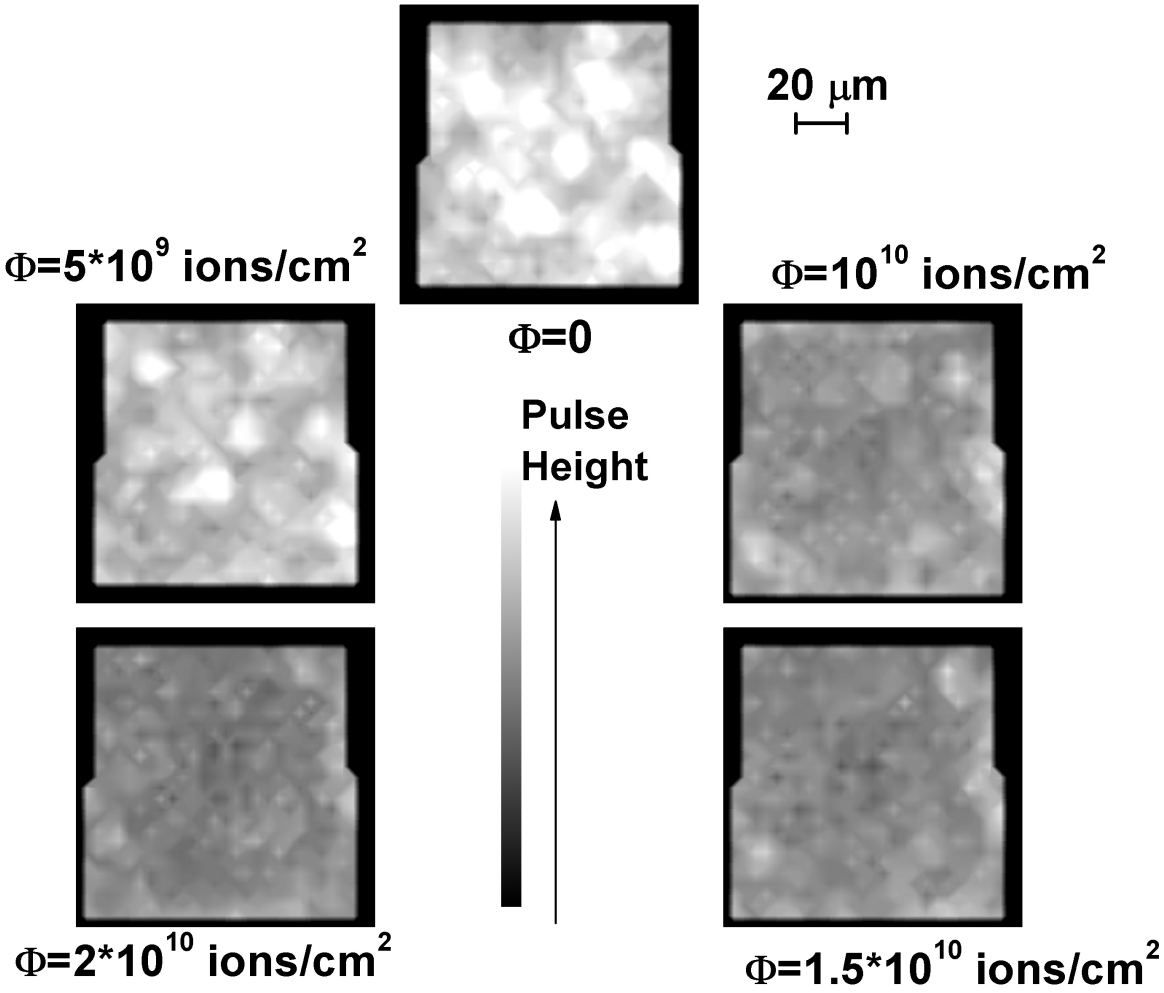
20 μm
Φ=5*10^9 ions/cm^2
Φ=10^10 ions/cm^2
Φ=0
Pulse
Height
Φ=2*10^10 ions/cm^2
Φ=1.5*10^10 ions/cm^2

Fig. 9